Comparison of Analytical Methodologies for Analysis of Single Sided Linear Permanent Magnet Flux Switching Machine: No-Load Operation

Noman Ullah [1,2], Muhammad Kashif Khan [2], Faisal Khan [1], Abdul Basit [2], Wasiq Ullah [1], Tanvir Ahmad [2], and Naseer Ahmad [1]

[1] Department of Electrical Engineering
COMSATS University Islamabad (Abbottabad Campus), Abbottabad, 22060, Pakistan
(nomanullah, faisalkhan)@ciit.net.pk

[2] U.S.-Pakistan Center for Advanced Studies in Energy
University of Engineering & Technology, Peshawar, 25000, Pakistan
(abdul.basit, tanvir.ahmad)@uetpeshawar.edu.pk, kashifkhanmarwat@yahoo.com

Abstract ─ A novel single sided Linear Permanent Magnet Flux Switching Machine (LPMFSM) with twelve mover slots and fourteen stator teeth (12/14), having two additional end teeth on both sides of mover is presented. Presence of both Armature Winding (AW) and Permanent Magnet (PM) on mover structure results in completely passive, robust, and low cost stator. While, demerits such as less slot area, complex flux density distribution, and magnetic saturation caused by passive stator demands to be analyzed by time consuming and computationally complex numerical modelling techniques, i.e., Finite Element (FE) Analysis, requiring expensive hardware/software. In this paper, two cost effective and fast response analytical techniques are developed to analyze no-load performance of LPMFSM. Two no-load characteristics, i.e., open-circuit flux linkage and detent force are analyzed by Equivalent Magnetic Circuit (termed as analytical technique No. 1) and Lumped Parameter Equivalent Magnetic Circuit (termed as analytical technique No. 2). Both analytical methodologies are compared and validated with corresponding globally accepted FE Analysis. Analysis revealed that LPEMC is better approach for initial design of LPMFSM.

Index Terms ─ Equivalent Magnetic Circuit, Finite Element Analysis, Linear Permanent Magnet Flux Switching Machine, Lumped Parameter Equivalent Magnetic Circuit.

I. INTRODUCTION

Rotary machines used for translational motion exhibit low efficiency and high cost due to requirement of sophisticated gear system for conversion of rotational torque to linear thrust force. Linear motors can provide direct linear thrust force, increased reliability due to reduction of mechanical conversion system, faster dynamic response, and good overload capability [1].

LPMFSM combines features of Linear Permeant Magnet Synchronous Machine (LPMSM) and Linear Switched Reluctance Machine with additional advantages of high power density [2], bipolar flux linkage, ability to re-magnetize PMs by changing the winding connections appropriately when PM performance is degraded, robust stator structure [3], lowered manufacturing cost [4], and compatibility with extreme environmental conditions due to better temperature control. LPMFSM can be used for long stroke applications such as rail transportation systems [5], short stroke oscillatory applications [6] such as rope-less elevators and long telescopes, and also as linear generator for wave energy extraction [7].

Numerous modelling techniques can be implemented for design and analysis of linear machines. These techniques can be enveloped as: (a) analytical, and (b) numerical techniques. Analytical techniques are preferred at initial design stage, and numerical methods are implemented for verification and refinement at the end of design process [8].

Limitations and demerits of LPMFSM such as complex mover structure and less slot area (due to presence of both PMs and armature windings), complex flux density distribution, and magnetic saturation caused by passive stator demands to be analyzed by time consuming and computationally complex numerical modelling techniques, i.e., FEA, requiring expensive hardware/software.

To increase computational ease, fast but accurate analytical modelling techniques are essential in the early development phase for the analysis and assessment of different concepts. Authors of [9] researched an analytical model based on formal solution of Maxwell's equations and examined open-circuit performance (cogging force, electromotive force, and iron losses) for Permanent Magnet Linear Machine (PMLM). Author

Submitted On: May 15, 2018
Accepted On: June 17, 2018

claimed about: (a) very good agreement of analytical model results with corresponding FEA results, and (b) reduction of computational time by almost six times required for FE Analysis. Three dimensional analytical magnetic charge model is implemented on transverse flux machine to minimize machine volume with fixed constraints on magnetic flux density and slot leakage, calculated propulsion force shows errors of only 8.9% to corresponding FE Analysis results [10]. On-load detent force calculations by considering magnetic saturation utilizing Frozen Permeability (FP) method is done in [11], and is validated by Maxwell Stress Tensor (MST) method and FE Analysis. Recently, authors of [12] researched an analytical method to calculate right/left detent end force of LPMSM, investigated novel technique to minimize fundamental and high-order harmonics of detent force, and finally analytical calculations are verified with experimental results.

However, literature about analytical techniques developed for LPMFSM is very limited ([13], [14]), and require immediate attention to enhance pre-design predictions. Authors of [13] combined response surface methodology with FE Analysis to calculate influence of design parameters on the LPMFSM net thrust force. Hybrid analytical approach based on strong coupling of EMC and formal solution of Maxwell's equations for LPMFSM to predict magnetic flux density, cogging force, and electromotive force is developed in [14].

In this paper, a novel single sided LPMFSM with twelve mover slots and fourteen stator teeth (12/14), having two additional end teeth on both sides of mover is developed and simulated for open-circuit flux linkage utilizing JMAG Commercial FEA Package v. 14. Objective of this paper is to develop and compare two different analytical techniques for LPMFSM to analyze no-load characteristics of LPMFSM. Design variables and dimensions of LPMFSM are presented in Section II. Operating principle of LPMFSM is discussed in Section III. Section IV explains division of LPMFSM into different equivalent circuit modules, i.e., stator, mover, PM, and air-gap. Solution methodologies used for two different analytical modelling techniques (EMC and LPEMC) is presented in Section V. Analytical techniques are compared with each other in terms of accuracy and validated with globally accepted FE Analysis in Section VI. Finally conclusions are drawn in Section VII.

II. DESIGN METHODOLOGY

Figure 1 shows a rotary twelve-stator-slot and ten-rotor-teeth (12/10) Permanent Magnet Flux Switching Machine (PMFSM) with trapezoidal armature coil slot structure. Its open-circuit flux linkage was investigated in [15], cogging torque and electromagnetic torque were also investigated. Results show that its open-circuit flux linkage is higher than that of 12/10 PMFSM with rectangular armature coil slot structure, when other machine design parameters (such as coil slot area, number of turns per phase, PM thickness, stack length etc.) are kept constant. Rotary 12/10 PMFSM is unrolled at position shown in Fig. 1 to obtain LPMFSM. Performance of initial design suffers from an unbalanced magnetic circuit, to compensate the problem two additional end teeth are added at both sides of mover as shown in Fig. 2. Unbalanced magnetic circuit can introduce significant detent force and contribute to thrust force ripples. Additional end teeth mitigates problem of unbalanced magnetic circuit and reduces detent force [16]. Design variables are depicted in Fig. 3, and dimensions are illustrated in Table 1.

III. OPERATING PRINCIPLE

Operating principle of LPMFSM is illustrated in Fig. 4. When relative position of stator poles and a particular mover tooth is (assuming $\theta_e = 0°$) as shown in Fig. 4 (a), the coil flux-linkage is assumed as positive maximum value. When the mover moves to position $\theta_e = 90°$ as shown in Fig. 4 (b), the flux linkage of coil approaches to zero value. Flux linkage in coil is assumed as negative maximum value (as shown in Fig. 4 (c)) after further 90° movement, i.e., $\theta_e = 180°$. When the mover moves by one stator pole pitch ($\theta_e = 270°$, Fig. 4 (d)), the flux linkage of coil again approaches zero value. Figure 4 (e) explains that idealized flux linkage of LPMFSM is bipolar.

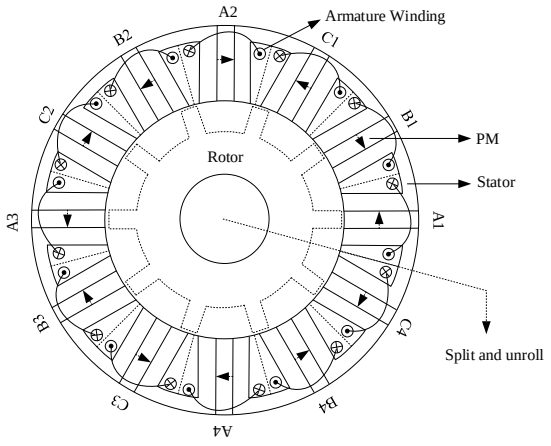

Fig. 1. Rotary 12/10 PMFSM.

IV. EQUIVALENT CIRCUIT MODULES

A. Air-gap equivalent circuit modules

In this paper, magnetic flux distribution within the region of air-gap between stator and mover is termed as air-gap Equivalent Circuit (EC). FE Analysis revealed that stator tooth position effects magnetic flux distribution within the air-gap region. To account air-gap magnetic flux distribution variation, multiple air-gap EC modules are modeled corresponding to different stator positions.

One mover pole pitch of 12/14 LPMFSM is modelled at different stator positions. Six different air-gap EC modules are constructed when one mover pole pitch covers linear displacement of one stator pole pitch.

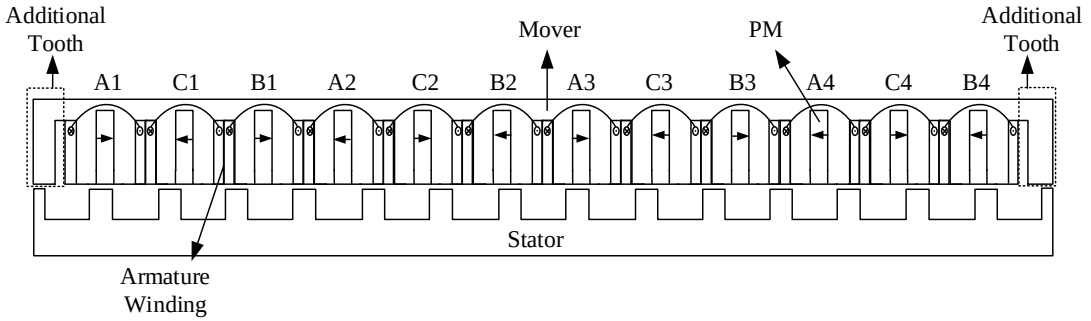

Fig. 2. Cross section of 12/14 LPMFSM.

As stator tooth enters different mover's position, different air-gap EC module is used with PM as its central axis. Due to periodic nature of LPMFSM (as illustrated in Section III), only six air-gap equivalent circuit modules are required.

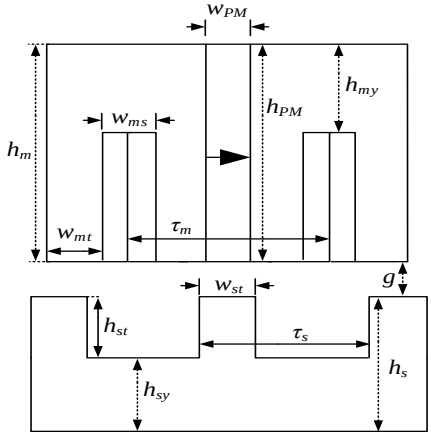

Fig. 3. Design parameters of mover and stator.

Flux lines follow specific paths to link between mover and stator, these paths are termed as Flux tubes [15, 17]. Six different flux tubes are observed during FE Analysis as shown in Fig. 5. Permeance of these flux tubes is calculated using formulas tabulated in Table 2 [17].

B. PM EC module

PM is modeled as Magnetomotive force ($\mathcal{F}_{\mathrm{PM}}$) source with permeance in series. Equation (1) is used to calculate $\mathcal{F}_{\mathrm{PM}}$:

$$\mathcal{F}_{PM} = \frac{B_r . w_{PM}}{\mu_0 \mu_r} . \quad (1)$$

C. Stator EC module

Unit section and its corresponding EC module of 12/14 LPMFSM stator is shown in Fig. 6 (a) and Fig. 6 (b). Branches of stator EC are illustrated by numbers, while nodes are introduced by alphabets. Permeance of stator back iron and stator tooth (P_{si} and P_{st}) are calculated using (2) and (3), respectively:

$$P(si) = \frac{\mu_0 \mu_r h_{sy} L}{t_s + h_{sy}} , \quad (2)$$

$$P(st) = \frac{\mu_0 \mu_r w_{st} L}{w_{st}} . \quad (3)$$

Table 1: Design dimensions of LPMFSM

Items	**Parameter**	**Unit**
Stator pole pitch $\boldsymbol{t_s}$	36	mm
Mover pole pitch $\boldsymbol{t_m}$	42	mm
Stack Length **L**	120	mm
Velocity $\boldsymbol{v}$	1.41	m/s
Mover tooth width $\boldsymbol{w_{mt}}$	10.5	mm
Stator tooth width $\boldsymbol{w_{st}}$	15.75	mm
Mover slot width $\boldsymbol{w_{ms}}$	10.5	mm
Mover back iron height $\boldsymbol{h_{my}}$	15.75	mm
Stator back iron height $\boldsymbol{h_{sy}}$	20	mm
Magnet width $\boldsymbol{w_{PM}}$	10.5	mm
Mover height $\boldsymbol{h_m}$	50	mm
Stator height $\boldsymbol{h_s}$	35	mm
Stator tooth height $\boldsymbol{h_{st}}$	15	mm
Magnet height $\boldsymbol{h_{PM}}$	10.5	mm
Air gap length $\boldsymbol{g}$	1	mm
PM remanence $\boldsymbol{B_r}$	1.2	T
PM relative permeability $\boldsymbol{\mu_r}$	1.05	-
Number of turn per coil $\boldsymbol{N_{coil}}$	116	-

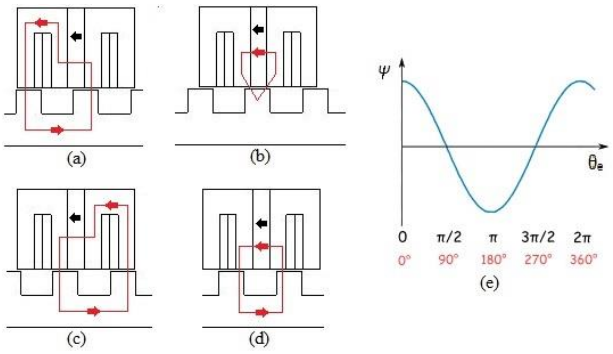

Fig. 4. Operating principle: (a) $\theta_e = 0°$, (b) $\theta_e = 90°$, (c) $\theta_e = 180°$, (d) $\theta_e = 270°$, and (e) Ideal flux linkage.

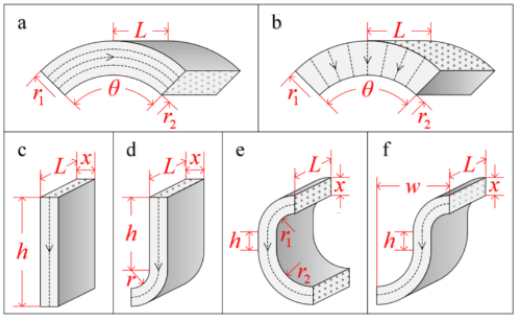

Fig. 5. Flux tubes obtained from FE Analysis.

Table 2: Permeance calculation formulas for flux tubes

Flux tube	Permeance	Flux tube	Permeance
a	$\frac{\mu L\theta}{\ln(\frac{r_2}{r_1})}$	d	$\frac{2\mu L.\ln\left(1+\frac{\pi x}{\pi r+2h}\right)}{\pi}$
b	$\frac{\mu L\ln(\frac{r_2}{r_1})}{\theta}$	e	$\frac{\mu L.\ln(1+\frac{2\pi x}{\pi r_1+\pi r_2+2h})}{\pi}$
c	$\frac{\mu Lx}{h}$	f	$\frac{2\mu Lx}{(\pi w+2h)}$

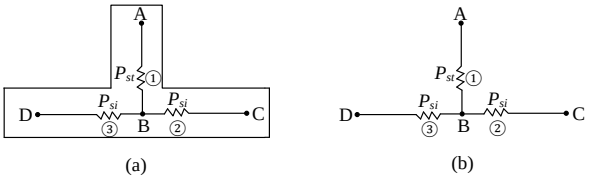

Fig. 6. Stator EC module: (a) stator section, and (b) EC of stator section.

D. Mover EC module

Unit section and its corresponding EC module of 12/14 LPMFSM mover is shown in Fig. 7 (a) and Fig. 7 (b). Branches of mover EC are illustrated by numbers, while nodes are introduced by alphabets. Permeance of mover back iron and mover tooth (P_{mi} and P_{mt}) are calculated using (4) and (5), respectively. Permeance of mover leakage (P_{ml}) is calculated using (6):

$$P(mi) = \frac{\mu_0\mu_r h_{my} L}{t_m + h_{my}}, \tag{4}$$

$$P(mt) = \frac{\mu_0\mu_r w_{mt} L}{w_{mt}}, \tag{5}$$

$$P(ml) = \frac{\mu_0 w_{PM} L}{t_m + w_{PM}}. \tag{6}$$

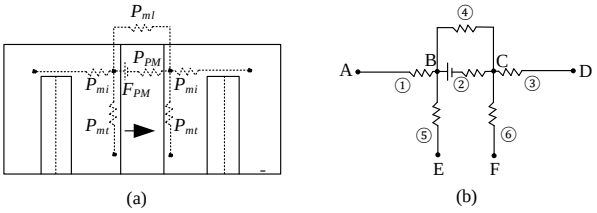

Fig. 7. Mover EC module: (a) mover section, and (b) EC of mover section.

V. SOLUTION METHODOLOGY

This section introduces features of incidence matrix and general equation utilized (for both analytical techniques) to compute magnetic potentials of each node and detent force. Mover, stator and air-gap EC modules are described as matrices, these matrices are merged and solved using incidence matrix method [18] utilizing MATLAB Software.

Incidence matrix A of a circuit having *x* nodes and *y* branches is *x* x *y* matrix, in which:

$$\boldsymbol{A}_{x,y} = \begin{cases} 0, & when\ branch\ y\ is\ not\ connected\ to\ node\ x, \\ -1, & when\ branch\ y\ ends\ to\ node\ x, \\ 1, & when\ branch\ y\ begins\ from\ node\ x. \end{cases} \tag{7}$$

Magnetic potentials of each node are calculated by using (8) that ultimately helps to compute magnetic flux through each flux tube [15]:

$$V = (\boldsymbol{A}.\boldsymbol{\Lambda}.\boldsymbol{A}^t)^{-1}.(\boldsymbol{A}.\boldsymbol{\Lambda}.\mathrm{E}), \tag{8}$$

where, E is mmf source in each branch (n x 1 vector), and Λ is n x n diagonal matrix representing permeance of each branch.

Equation (9) is generalized form of MST method and is used to compute detent force of LPMFSM by extracting radial and axial component of magnetic flux density from FE Analysis:

$$F_x = \frac{GCD(N_{ms}, N_{sp}).L}{\mu_0} \int_0^{L_{Perp}} B_x(x,y).B_y(x,y).dx, \tag{9}$$

where, N_{ms} is number of mover slots, N_{sp} is number of stator teeth, and L_{Perp} is axial length in x-direction.

A. Equivalent magnetic circuit

In this paper, EMC methodology accounts six different air-gap equivalent circuit modules (termed as Segment No. 1 - 6) and does not account permeances of mover and stator equivalent modules for node potential calculations. Reluctance/Permeance network for Phase "C" of 12/14 LPMFSM is shown in Fig. 8 (a). Permeances of different types of flux tubes identified for Segment No. 1 – Segment No. 6 are tabulated in Table 3. Reluctance network of 12/14 LPMFSM air-gap EC modules corresponding to six different stator segments is generated and solved for magnetic potentials using (8). Equation (9) is used to compute detent force by extracting air-gap magnetic flux density (as shown in Figs. 9 (a-b)) from FE Analysis.

B. Lumped parameter equivalent magnetic circuit

Lumped parameter reluctance network of LPMFSM's consists of six air-gap EC modules (illustrated in Table 3), fourteen stator EC modules (Fig. 6 (b)), and twelve mover EC modules (Fig. 7 (b)). Permeance of stator back iron and stator tooth is calculated using (2) and (3), respectively. Permeance of mover back iron, mover tooth, and mover leakage is calculated using (4), (5), and (6), respectively.

Table 3: Types of flux tubes in six different air-gap EC modules

Segment Number	Flux Tube Number								
	1	**2**	**3**	**4**	**5**	**6**	**7**	**8**	**9**
1	d	d	b	d	c	d	d	c	d
2	d	c	d	f	d	c	d	d	-
3	d	d	c	d	f	d	c	d	-
4	d	c	d	b	d	d	d	d	b
5	d	d	d	b	d	c	d	d	-
6	b	d	c	d	d	d	d	c	-

Reluctance/Permeance network for Phase "C" of 12/14 LPMFSM is shown in Fig. 8 (b) which clearly indicates that LPEMC methodology accounts stator back iron and teeth, mover back iron, teeth, and leakage, and air-gap EC modules. Magnetic potential calculations are done using (8). Equation (9) is used to compute detent force by extracting mover teeth magnetic flux density (as shown in Figs. 9(c-d)) from FE Analysis.

VI. COMPARISON OF ANALYTICAL TECHNIQUES

Open-circuit flux linkage obtained for mover pole pitch from analytical modelling techniques (EMC and LPEMC) are compared with globally accepted FE Analysis results in Fig. 10 (a) and Fig. 10 (b), respectively. Point-to-point percentage error is shown in Fig. 11 (a). Analysis of open-circuit flux linkage of reveals that EMC methodology suffers with errors less than ~8.5%, while LPEMC methodology shows errors less than ~7.5%. Peak-to-peak open-circuit flux linkage obtained by analytical methodologies (EMC and LPEMC) and FE Analysis is shown in Fig. 11 (b).

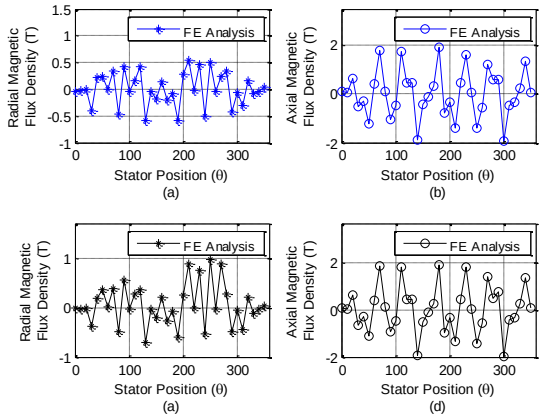

Fig. 9. FE Analysis magnetic flux densities: (a) air-gap radial component, (b) air-gap axial component, (c) mover radial component, and (d) mover component.

Detent force for periodic boundary of one mover pole pitch is also computed by EMC and LPEMC methodology, and compared with corresponding FE Analysis results in Fig. 12 (a) and Fig. 12 (b), respectively. Point-to-point percentage error of detent force is shown in Fig. 13 (a), and reveals that EMC methodology suffers with errors less than ~18%, while LPEMC methodology shows errors less than ~14.5%. Average detent force obtained by analytical methodologies (EMC and LPEMC) and FE Analysis is shown in Fig. 13 (b). Limitations of analytical methodologies are: (a) does not account magnetic saturation, (b) permeability of iron core is assumed to be infinite, and (c) analytical methodologies provide shuffled values of calculated quantities and sorting must be done to compare wave-forms.

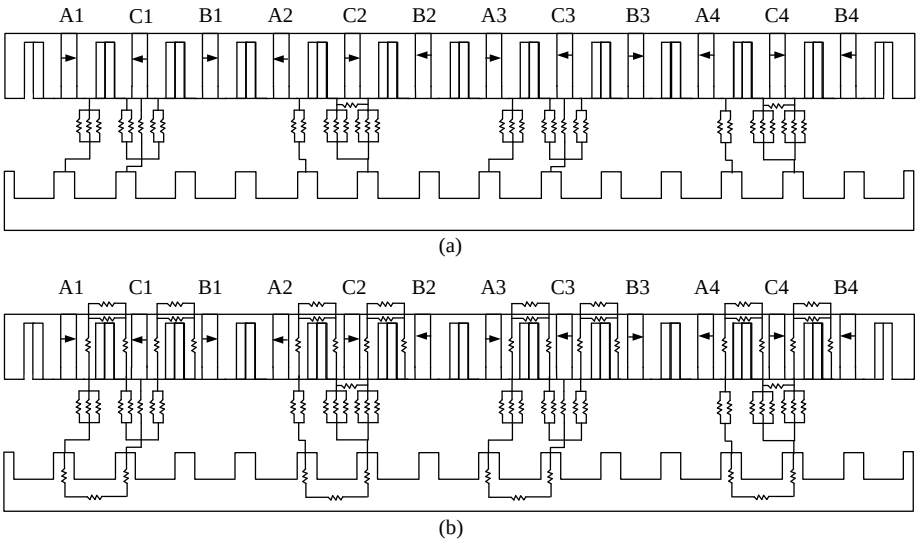

Fig. 8. Phase C reluctance/permeance network: (a) EMC and (b) LPEMC.

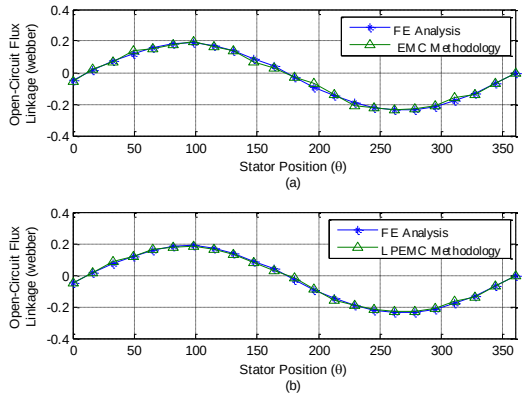

Fig. 10. Open-circuit flux linkage: (a) comparison of FE Analysis and EMC, and (b) comparison of FE Analysis and LPEMC.

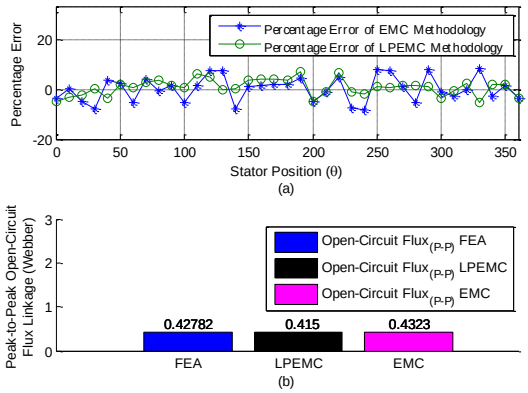

Fig. 11. Open-circuit flux linkage: (a) point-to-point percentage error, and (b) peak-to-peak open-circuit flux linkage.

VII. CONCLUSION

Aim of this paper is to simulate novel single sided LPMFSM using JMAG Commercial FEA Package v. 14, develop two analytical modelling techniques for prediction of no-load characteristics, i.e., open-circuit flux linkage and detent force, and compare both analytical methodologies with corresponding globally accepted FE Analysis results. Analytical technique No. 1 (EMC) represents peak error of less than ~8.5% for open-circuit flux linkage and ~18% for detent force, while analytical technique No. 2 (LPEMC) represents peak error of less than ~7.5% for open-circuit flux linkage and ~14.5% for detent force. This paper validates both analytical techniques and made authors to recommend LPEMC approach for initial design of LPMFSM.

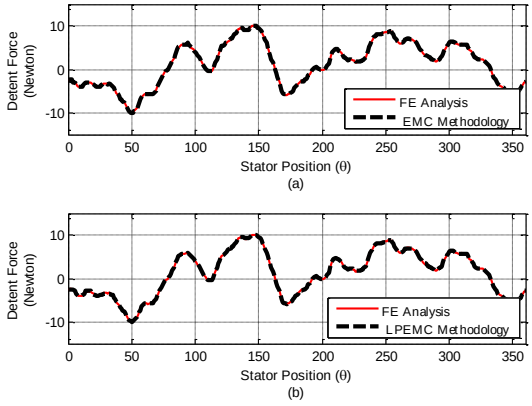

Fig. 12. Detent force: (a) comparison of FE Analysis and EMC, and (b) comparison of FE Analysis and LPEMC.

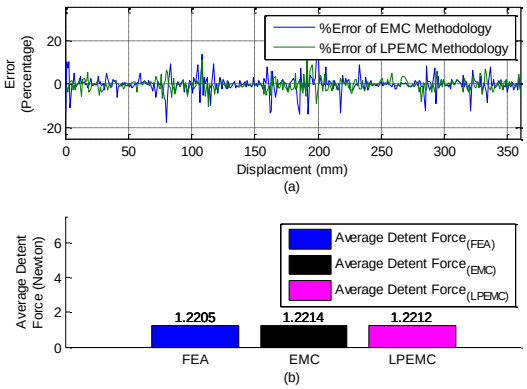

Fig. 13. Detent force, (a) point-to-point percentage error, and (b) average detent force.

REFERENCES

[1] J. F. Gieras and Z. J. Piech, *Linear Synchronous Motors: Transportation and Automation Systems*. Boca Raton, FL, USA: CRC, 2000.

[2] C. F. Wang, J. X. Shen, Y. Wang, L. L. Wang, and M. J. Jin, "A new method for reduction of detent force in PM flux-switching linear motors," *IEEE Trans. Magn.*, vol. 45, no. 6, pp. 2843-2846, 2009.

[3] J. Ou, Y. Liu, M. Schiefer, and M. Doppelbauer, "A novel PM-free high-speed linear machine with amorphous primary core," *IEEE Trans. Magn.*, vol. 53, no. 11, 2017.

[4] C. Hwang, P. Li, and C. Liu, "Design and analysis of a novel hybrid excited linear flux switching permanent magnet motor," *IEEE Trans. Magn*., vol. 48, no. 11, pp. 2969-2972, Nov. 2012.

[5] R. Cao, M. Cheng, C. Mi, W. Hua, X. Wang, and W. Zhao, "Modeling of a complementary and modular linear flux-switching permanent magnet motor for urban rail transit applications," *IEEE Trans. Energy Convers*., vol. 27, no. 2, pp. 489-497, June 2012.

[6] A. Gandhi and L. Parsa, "Thrust optimization of a flux-switching linear synchronous machine with yokeless translator," *IEEE Trans. Magn.*, vol. 49, no. 4, pp. 1436-1443, Apr. 2013.

[7] L. Huang, H. Yu, M. Hu, J. Zhao, and Z. Cheng, "A novel flux-switching permanent-magnet linear generator for wave energy extraction application," *IEEE Trans. Magnetics*, vol. 47, pp. 1034-1037, 2011.

[8] S. Ouagued, Y. Amara, and G. Barakat, "Comparison of hybrid analytical modelling and reluctance network modelling for predesign purposes," *Mathematics and Computers in Simulation*, vol. 130, pp. 3-21, 2016.

[9] Y. Laoubi, M. Dhifli, G. Verez, Y. Amara, and G. Barakat, "Open circuit performance analysis of a permanent magnet linear machine using a new hybrid analytical model," *IEEE Trans. Magn.*, vol. 51, no. 3, Mar. 2015.

[10] M. F. J. Kremers, J. J. H. Paulides, and E. A. Lomonova, "Toward accurate design of a transverse flux machine using an analytical 3-D magnetic charge model," *IEEE Trans. Magn.*, vol. 51, no. 11, Nov. 2015.

[11] Y. Yao, Q. Lu, X. Huang, and Y. Ye, "Fast calculation of detent force in PM linear synchronous machines with considering magnetic saturation," *IEEE Trans. Magn.*, vol. 53, no. 6, June 2017.

[12] H. Hu, X. Liu, J. Zhao, and Y. Guo, "Analysis and minimization of detent end force in linear permanent magnet synchronous machines," *IEEE Trans. Industrial Electronics*, vol. 65, no. 3, Mar. 2018.

[13] B. Zhang, M. Cheng, R. Cao, Y. Du, and G. Zhang, "Analysis of linear of flux-switching permanent-magnet motor using response surface methodlogy," *IEEE Trans. Magn.*, vol. 50, no. 11, Nov. 2014.

[14] Y. Laoubi, M. Dhifli, G. Barakat, and Y. Amara, "Hybrid analytical modeling of a flux switching permanent magnets machines," *International Conference on Electrical Machines (ICEM)*, pp. 1018-1023, 2014.

[15] N. Ullah, F. Khan, W. Ullah, M. Umair, and Z. Khattak, "Magnetic equivalent circuit models using global reluctance networks methodology for design of permanent magnet flux switching machine," *15th International Bhurban Conference on Applied Sciences and Technology (IBCAST)*, pp. 397-404, 2018.

[16] C. Wang, J. Shen, Y. Wang, L. Wang, and M. Jin, "A new method for reduction of detent force in permanent magnet flux-switching linear motors," *IEEE Trans. Magn.*, vol. 45, no. 6, pp. 2843-2846, June 2009.

[17] V. Ostovic, *Dynamics of Saturated Electric Machines*. Berlin Heidelberg, Germany: Springer-Verlag New York Inc., 1989.

[18] L. O. Chuaand and P. M. Lin, *Computer-Aided Analysis of Electronic Circuits-Algorithms and Computational Techniques*. Prentice Hall, Englewood Cliffs, NJ, USA, 1975.

Noman Ullah received his B.Sc. and M.Sc. degree in Electrical (Power) Engineering from University of Engineering & Technology, Peshawar, Pakistan in 2012 and 2015, respectively. He is working as Lecturer at COMSATS University Abbottabad, Pakistan. He is Reviewer of IEEE

Transactions on Transportation Electrification. His research interests includes analytical modelling of electrical machines.

Faisal Khan received his Ph.D. Electrical Engineering degree from Universiti Tun Hussein Onn Malaysia in 2016. He is working as Assistant Professor at COMSATS University Abbottabad, Pakistan.

Abdul Basit received his Ph.D. from the Department of Wind Energy of the Technical University of Denmark in 2015. Basit is currently employed as an Assistant Professor at UET Peshawar, Pakistan.

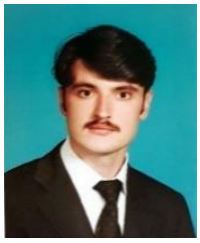

Wasiq Ullah received his B.Sc. degree in Electrical (Power) Engineering from COMSATS University Abbottabad, Pakistan in 2018 and currently enrolled as M.Sc. Electrical (Power) Engineering student from COMSATS University Abbottabad, Pakistan. He is working as Research Member with Electrical Machine Design Group.

Naseer Ahmad received his Bachelor degree in Electrical (Power) Engineering in 2015 from University of Engineering and Technology, Peshawar, Pakistan and currently enrolled as M.Sc. Electrical (Power) Engineering student form COMSATS University Abbottabad, Pakistan.